Polymer 51 (2010) 4390–4397

Contents lists available at ScienceDirect

Polymer

journal homepage: www.elsevier.com/locate/polymer

Variations in cross-link density with deposition pressure in ultrathin plasma polymerized benzene and octafluorocyclobutane films

Someswara R. Peri [a], Brian Habersberger [a], Bulent Akgun [b,c], Hao Jiang [d], Jesse Enlow [d], Timothy J. Bunning [d], Charles F. Majkrzak [b], Mark D. Foster [a,*]

[a] Department of Polymer Science, The University of Akron, 170 University Ave., Akron, OH 44325-3909, USA
[b] NIST Center for Neutron Research, Gaithersburg, MD 20899, USA
[c] Department of Materials Science and Engineering, University of Maryland – College Park, MD 20742, USA
[d] Air Force Research Laboratory, Materials and Manufacturing Directorate, Wright-Patterson Air Force Base, OH 54333, USA

ARTICLE INFO

Article history:
Received 21 February 2010
Received in revised form
15 July 2010
Accepted 17 July 2010
Available online 24 July 2010

Keywords:
Plasma enhanced chemical vapor deposition
Cross-link density
Neutron reflectometry

ABSTRACT

Neutron reflectometry (NR) measurements of ultrathin films from octafluorocyclobutane (OFCB) and benzene (B) precursors deposited using Plasma Enhanced Chemical Vapor Deposition (PECVD) at two pressures (0.6 and 0.05 torr) reveal that under both deposition conditions there are a 7 nm-thick surface layer and an approximately 1 nm-thick transition layer next to the substrate which have structures different than those in the middle of the film. NR measurements of films swollen with solvent reveal that the density of cross-linking next to the substrate is lower than that in the middle of the film or the region adjacent to the surface of the film for both precursors. Variations in the cross-link density with processing pressure are much stronger for PP-B films than for PP-OFCB films.

1. Introduction

Thin films exhibiting highly cross-linked structures have been targeted for applications such as waveguides, passive filters and capacitors for dielectric devices [1–4]. Plasma polymerized (PP) films have attracted recent interest due to their properties including insolubility, good adhesion to substrates, high cross-linking density, and a smooth and pin-hole free structure [5–7]. Although there have been some studies of the structure within these PP films [8–10], a more fundamental understanding of the film structure, especially the establishment of structure-property relationships, is critical for finding optimum designs for various optical and dielectric applications.

Using a single precursor (monomer), it is possible to obtain films with a variety of structures simply by varying the deposition conditions, and it is therefore advantageous to understand how the processing conditions define the structure and properties of such films. Previously, Kim et al. [9] found that films of plasma polymerized homopolymers of benzene and octafluorocyclobutane (OFCB) precursors of thickness 25–40 nm processed at 30 W plasma power and 0.6 torr reactor pressure had extremely smooth interfaces and structures that were uniform through the depth of the film. The only variation in structure with depth reported was associated with a very thin (ca. 1 nm) transition layer next to the substrate for films made from OFCB (PP-OFCB). The current contribution addresses how the structure of 10–20 nm thick PP-homopolymer films changes when the reactor pressure is varied, and how the cross-link density varies with depth for the processing conditions studied. In these ultrathin films, interfacial structure is the dominant feature of film structure.

Jeon and coworkers [10] studied variations with depth in cross-link density for PP-(methyl methacrylate) (PMMA) homopolymer films deposited at 60 W plasma power by collecting neutron reflectivity (NR) data for the 20–140 nm thick films after swelling with good solvent-vapor. They reported that the cross-link density was uniform from the substrate surface to the air interface. Nelson and coworkers [8] reported that PP-allylamine (AA) and PP-hexamethyldisiloxane (HMDS) homopolymer films, deposited at a plasma power of 10 W and then swollen with water, swelled to different extents. The hydrophilic PP-AA swelled four times as much as the hydrophobic PP-HMDS. No indication of variation in cross-link density through the film was reported.

The present contribution focuses on the role of pressure on the dry and swollen interface structure of ultrathin (<20 nm) PP-OFCB and PP-Benzene (PP-B) films deposited at 45 W in contrast to the thicker films deposited at 30 W power that were studied by Kim et al. [9]. The differences in the structure with processing

* Corresponding author. Tel.: +1 330 972 5323; fax: +1 330 972 5290.
E-mail address: mfoster@uakron.edu (M.D. Foster).

0032-3861/$ – see front matter © 2010 Elsevier Ltd. All rights reserved.
doi:10.1016/j.polymer.2010.07.026

conditions are studied using NR, which is sensitive to film thickness, composition and density and to interface roughness [11–16]. NR measurements on dry PP-OFCB and PP-B films show a surface layer with lower scattering length density than the bulk, and in some cases a very thin transition region at the substrate. Measurements of swollen PP-OFCB and PP-B films show that solvent concentration is higher at the substrate than in the middle of the film or "surface", revealing that cross-link density varies with depth inside the film. Details of the film structure vary with reactor pressure, more so for PP-B films than for PP-OFCB films.

2. Materials and methods

PP-B films were made from the vapor of HPLC grade liquid benzene (C_6H_6) supplied by Aldrich [17]. PP-OFCB films were made from compressed OFCB supplied by SynQuest Laboratories [17]. The monomers were 99% pure and no additional purification steps were performed. The reactor used was similar to that used by Grant and coworkers [3]. Plasma power, argon flow rate, downstream monomer feed location (DS) and monomer flow rate were kept constant for the samples considered here. Plasma power was 45 W. Ar flow rate was 100 cc/min and the monomer feed rates were 3 cc/min for OFCB and 0.3 cc/min for benzene. Films were deposited on 3″ diameter silicon wafers for XPS and NR analysis. One PP-OFCB film (denoted "H-F") was deposited in the "high" pressure regime at a reactor pressure of 0.6 torr and another ("L-F") at a "low" reactor pressure of 0.05 torr. PP-B films were also deposited at each of these two reactor pressures and labeled "H-B" and "L-B".

Surface compositions were determined using XPS with an incident angle of 30° with respect to the sample surface on a Surface Science Instruments [17] M-probe spectrometer equipped with a monochromatic Al K_α source. The penetration depth of the X-rays was 5 nm at this incident angle. Survey scans covering binding energies of 0–1000 eV were made using an X-ray power of 200 W and analyzer pass energy of 150 eV. The spectrometer resolution was 1.5 eV and the analysis area was approximately 400 μm × 1000 μm.

Specular NR was measured at the National Institute of Standards and Technology (NIST) Center for Neutron Research on the NG1 reflectometer ($\lambda = 0.475$ nm). The intensity of reflected neutrons was measured as a function of momentum transfer vector in the direction normal to the surface q_z ($=4\pi sin\theta/\lambda$), which is a function of incident angle (θ). Data were collected with approximately fixed relative resolution ($\Delta q/q \approx 0.02$) by increasing the sizes of collimating and detector slits with increasing incident angle. The reflectivity was first measured on as-deposited samples, and then on samples swollen with good solvent-vapor. Either d-THF, a good solvent for PP-OFCB, or d-toluene, a good solvent for PP-B, was placed in a reservoir inside the NR sample chamber and the reflectivity measured after the sample had been exposed to solvent-vapor for 12 h (Measurements of the kinetics of swelling with other samples indicated that the equilibrium was reached on a time scale of 3 h).

The property of the films to which NR is sensitive is the scattering length density (SLD), or $(b/V)_n$. The value of $(b/V)_n$ can be related to the molecular properties of the film by

$$(b/V)_n = \frac{N_A \rho_b \sum b_i}{MW} \quad (1)$$

where MW is the molar mass of a representative "repeat unit" of the polymer, ρ_b is the mass density in the volume of interest, b_i is the scattering length of element i in the repeat unit, the sum is over all atoms in the repeat unit, and N_A is Avogadro's number. Thus $(b/V)_n$ varies as a function of both the mass density of the film and the composition in the film. If phase-sensitive methods employing reference layers or variation of the surrounding media cannot be performed for technical reasons [18], then the sample neutron SLD cannot be obtained directly from NR data because of the loss of phase information, but must be obtained by a fitting procedure [19]. A candidate model is assumed for the film structure and the model parameters are varied until good agreement between the simulated reflectivity and data is achieved. The model SLD profile is created by first approximating the structure as a stack of fictitious layers, each of which has thickness d and uniform scattering length density $(b/V)_n$. Each of the interfaces in the sample, including the interface between the substrate and film, the interface between film and air, and the interface between each pair of layers in the film, is convoluted with an appropriate error function to represent the full effective width of the interface, the width of each interface being parameterized by a value of σ for that error function. This effective width includes both the effect of roughness as well as the intrinsic width of the interface, since reflectivity experiments only measure the one-dimensional SLD profile as a function of depth. The simulated model reflectivity was calculated using the Parratt formalism [20] and values of the model parameters obtained using a nonlinear least squares regression of the data.

3. Results and discussion

3.1. As-deposited structure – benzene monomer

Fig. 1 shows the neutron reflectivity data and the best fit for PP-B films deposited in the high and low pressure regimes. The most evident difference between the reflectivity curves is the difference in spacing of the interference fringes indicative of the film thicknesses. The fringes in the reflectivity curves for both samples propagate to the highest accessible values of q_z, indicating that the air interfaces are sharp. Parameters of the film structure in each sample are given in Table 1. In both cases, good fits with a figure of merit, χ^2, less than 1.4, were obtained. The SLD profiles corresponding to the best fit curves for the samples are shown in Fig. 2. In general, SLD model profiles were constructed using three layers in the underlying "box-like" model. The layer next to the substrate is denoted as the "bottom" or "transition" layer. We use the term "transition" layer for a layer that is comparatively thin and which

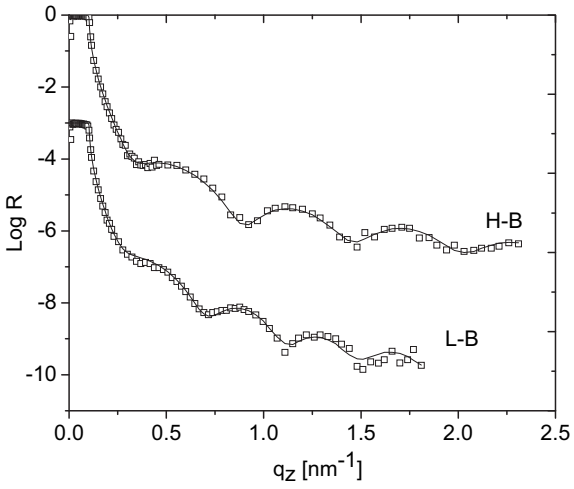

Fig. 1. NR data (symbols) and the best fit model reflectivity (line) for PP-B single layer films deposited at high pressure (H-B) and low pressure (L-B). The curves for the L-B film are shifted for clarity. Error bars in reflectivity figures are smaller than the size of data symbols.

Table 1
Model parameters for films deposited from benzene at different pressures.

Model Layer	Parameter	0.6 torr	0.05 torr
SiO_x	σ (nm) ± 10–15%	0.13	0.2
	$(b/V)_n \pm 0.1$ (10^{-4} nm^{-2})	3.27	2.97
	d (nm) ± 0.2 nm	0.6	0.7
Transition layer	σ (nm) ± 10–15%	1.5	1.5
	$(b/V)_n \pm 0.1$ (10^{-4} nm^{-2})	0.97	2.0
	d (nm) ± 0.2 nm	3.1	3.8
Middle layer	σ (nm) ± 10–15%	–	0.96
	$(b/V)_n \pm 0.1$ (10^{-4} nm^{-2})	–	1.03
	d (nm) ± 0.2 nm	–	2.6
Surface layer	σ (nm) ±10–15%	0.29	0.82
	$(b/V)_n \pm 0.1$ (10^{-4} nm^{-2})	0.65	0.6
	d (nm) ± 0.2 nm	8.1	6.9

lies underneath an abrupt increase in (b/V). For convenience the layer in the middle of the film is denoted as the "middle" layer and that next to the air as the "surface" layer. However, a "transition" layer was not needed for every model. This fictitious profile of box-like components is then modified by convoluting the interfaces with error function of appropriate widths. In comparing the structures of different films it is best to recall that while the uniform layer parameter values and interface widths summarized in the table provide some idea of differences among the structures of the samples, the true shapes of the profiles can only be appreciated by looking at the final SLD plots. The peak on the left of each SLD profile corresponds to the SiO_x layer atop the Si substrate. The PP-B film itself starts to the right of the SiO_x layer in the SLD profile. For PP-B films only two layers were needed for the film deposited at higher pressure, while three were required for the film deposited at lower pressure. The film deposited at higher pressure was not thick enough for a middle layer structure to develop.

For both deposition pressures, the structures of PP-B films vary substantially with depth (in contrast to the PP-OFCB films discussed later). Near the substrate, the SLD drops substantially over a very thin region followed by smaller, more gradual decreases through the total thickness. We note that this is fundamentally different than for PP films formed at 30 W from deuterated benzene (PP-dB) by Kim [9] and benzene (PP-B) by Peri [21]. XR of these PP-B ultrathin films deposited at 45 W (not shown) exhibit key features consistent with the NR data, i.e. strong variations in $(b/V)_x$ with depth, and apparent densities much lower than those of films deposited at 30 W. Thus, it seems that the transition in structure at the substrate appears upon the increase of deposition power from 30 W to 45 W.

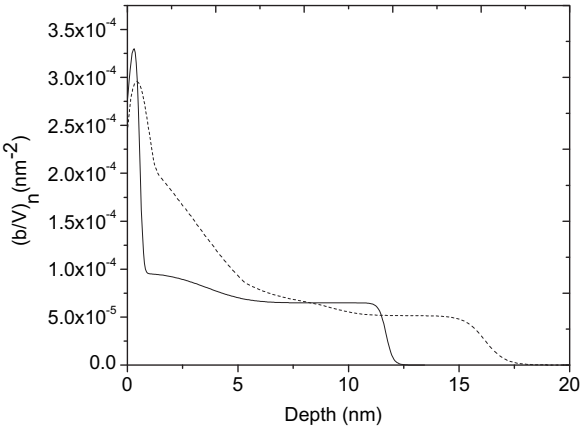

Fig. 2. $(b/V)_n$ Models for PP-B samples deposited at 0.6 torr (solid line) and 0.05 torr (dashed line). Zero on the depth scale is taken as the center of the interface between the Si substrate and its oxide layer.

The SLD profiles in Fig. 2 also reveal that the rms roughness of the polymer–air interface is greater for the film deposited at 0.05 torr (0.82 nm) than for the film deposited at 0.6 torr (0.29 nm). We conjecture that under the conditions of higher deposition rate (0.05 torr samples), there is not enough time for incoming fragments to diffuse laterally on the surface to achieve optimal smoothing of the new surface.

Finally, we see that the composition near the air interface is different from that of the composition in the interior of the film. This "surface layer" again appears here for films formed at 45 W, while it was not seen [9,21] for PP-dB and PP-B films deposited at 30 W. The region of reduced scattering length density next to the air surface has about the same thickness, ca. 7 nm, for the depositions at the two pressures. Since both films are ultrathin, the result of having both a ca. 3.5 nm thick "transition" layer and a surface layer of 7 nm is a SLD profile that is markedly non-uniform with depth. XPS analysis also showed that both films had an oxygen composition of 4 atom% at the surface, which is notable because the monomer contains no oxygen. Several studies [22–28] have pointed out that plasma polymerized films contain residual free radicals and dangling bonds that can form active oxidization centers [29–32]. Jiang and coworkers [33] reported 4 atom% oxygen on the surface of PP-B films (deposited at the same conditions of 45 W plasma power, 0.05 torr chamber pressure and argon flow rate of 10 cc/min) and there was a large concentration of free residual radicals within the films. Their XPS results also showed that the oxygen was confined primarily to the surface region, consistent with the contention that the oxygen diffuses into the film when exposed to ambient conditions. Swelling measurements discussed below show how the cross-linking density varies with depth in the films.

3.2. As-deposited structure – OFCB monomer

Fig. 3 shows the NR data and best fit curves for PP-OFCB samples deposited at 0.6 torr and 0.05 torr using OFCB monomer. The film characteristic of central interest is the uniformity of SLD with depth. Parameters of the film structure for each sample corresponding to the best fit are given in Table 2 and the SLD profiles are shown in Fig. 4. In contrast to the case of the PP-B films, the SLD profiles of the PP-OFCB films seem unaffected by deposition pressure aside from a change in deposition rate (i.e. if the deposition

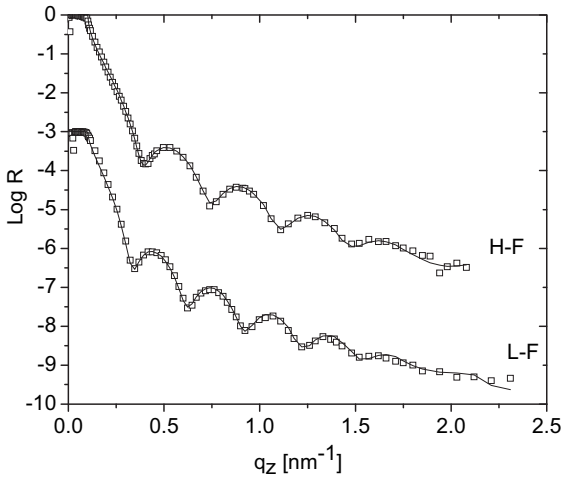

Fig. 3. NR data (symbols) and the best fit model reflectivity (line) for PP-OFCB films deposited at 0.6 torr pressure (H-F) and 0.05 torr pressure (L-F). The curves for L-F are shifted for clarity.

Table 2
Model parameters for films deposited at different pressures using OFCB monomer.

Model Layer	Parameter	0.6 torr	0.05 torr
SiO_x	σ (nm) ± 10–15%	0.32	0.3
	$(b/V)_n \pm 0.1$ (10^{-4} nm^{-2})	3.25	3.25
	d (nm) ± 0.2 nm	0.77	0.72
Transition layer	σ (nm) ± 10–15%	0.12	0.22
	$(b/V)_n \pm 0.1$ (10^{-4} nm^{-2})	2	2.3
	d (nm) ± 0.2 nm	0.3	0.3
Middle layer	σ (nm) ± 10–15%	3.5	3.5
	$(b/V)_n \pm 0.1$ (10^{-4} nm^{-2})	3.6	3.7
	d (nm) ± 0.2 nm	9.7	13.3
Surface layer	σ (nm) ± 10–15%	0.49	0.35
	$(b/V)_n \pm 0.1$ (10^{-4} nm^{-2})	3.2	3.2
	d (nm) ± 0.2 nm	7.0	6.9

times for the two films depicted in Fig. 4 had been chosen to achieve exactly equal overall thicknesses, the two SLD profiles would be very similar). The SLD profiles of both films show "transition layers" at the substrate and a surface layer of lower SLD.

An important difference between the structure of the PP-OFCB film deposited at 45 W reported here and that of the film deposited at 30 W reported earlier by Kim and coworkers [9] is the "surface layer" seen here. The "surface" layer of approximately 7 nm thickness is seen in both OFCB and benzene films, suggesting that its existence is not primarily dictated by details of the chemistry, but is instead a general feature of the deposition mechanism. The origin of the "surface" layer is probably through post-deposition reactions between residual radicals/dangling bonds near the film surface and moisture and oxygen in the air upon exposure to an ambient atmosphere, Although the electronegative fluorine on the PP-OFCB film surface strongly repels oxygen [34], sufficient oxygen (0.9 atom%) is incorporated to create a surface layer due to the large number of residual free radicals.

We note a difference in the sensitivity of the surface roughness to deposition pressure for PP-B and PP-OFCB films. While the roughness of the PP-B films changed markedly with deposition pressure, the roughness of the PP-OFCB films did not. They were 0.35 nm for the film deposited at 0.05 torr and 0.49 nm for the film deposited at 0.6 torr, a difference at the edge of our estimated uncertainties. We conjecture that this insensitivity to pressure is connected with the fact that while the deposition rate for PP-B films changed by 400% with the pressure increase from 0.05 to 0.6 torr, the deposition rate for PP-OFCB films changed by only 40%.

3.3. Cross-link density comparisons – benzene monomer

After swelling to equilibrium in d-toluene vapor, the PP-B film thickness increases dramatically and the fringes become very poorly defined as shown in Fig. 5, indicating that the roughnesses of the interfaces responsible for the fringes increase with swelling. Best fits to the data from the swollen PP-B films are shown in Fig. 5 and the corresponding SLD profiles are shown in Figs. 6 and 7. The fits to the data for swollen films were done assuming the amount of solvent in the film implied by the change in overall thickness must be consistent with the amount of solvent implied by the increase in b/V integrated over the thickness of the film, assuming ideal mixing.

The SLD profile for the swollen H-B film reveals a broad region with high $(b/V)_n$ near the substrate. For both films, this SLD in the swollen sample is much higher than the SLD in the as-deposited sample because the SLD of d-toluene (5.66×10^{-4} nm^{-2}) is much larger than the SLD of the dry polymer ($\sim 1.1 \times 10^{-4}$ nm^{-2}). Comparing the thicknesses of the dry and swollen films shows that the PP-B films swelled by a factor of three. Comparing the $(b/V)_n$ of pure solvent and that present in the swollen film, one can infer that this layer adjacent to the substrate contains about 90% solvent, so the cross-link density in the transition layer is low. Progressing upward toward the air interface, $(b/V)_n$ decreases monotonically, indicating that the film is increasingly more cross-linked towards the outer surface. However, not much can be said about cross-linking right at the air interface because the SLD reaches zero after passing the polymer–air interface. It is also possible that after swelling, the interface gets very rough, and the broad interface profile next to the air results from a combination of continuous change in cross-link density with depth and the increased roughness.

Both of the films show gradients in swelling with depth; however, for the PP-B film deposited at 0.05 torr, the value of $(b/V)_n$ peaks at the substrate interface and immediately begins to decrease in the direction of the air interface. For the film deposited at 0.6 torr, $(b/V)_n$ remains high near the substrate over some depth, and then decreases as one moves up toward the surface. Further analysis of the SLD profiles from the swollen films allows one to draw conclusions on the variations in cross-link density with depth. The central result is that, for both PP-B and PP-OFCB films, the cross-link density is lower at the oxide-interface than in either the middle of the film or at the air-interface.

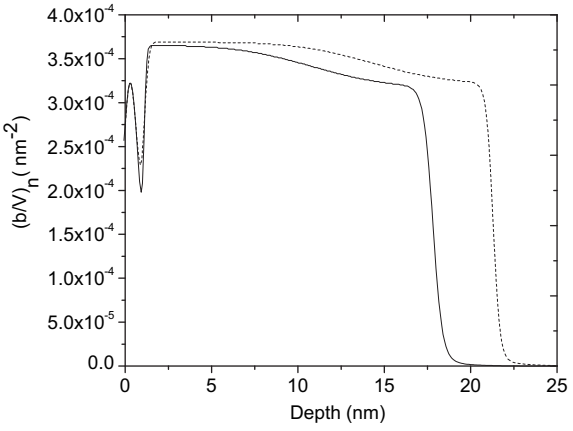

Fig. 4. $(b/V)_n$ Models for PP-OFCB samples deposited at 0.6 torr (solid line) and 0.05 torr (dashed line). Zero on the depth scale is taken as the center of the interface between the Si substrate and its oxide layer.

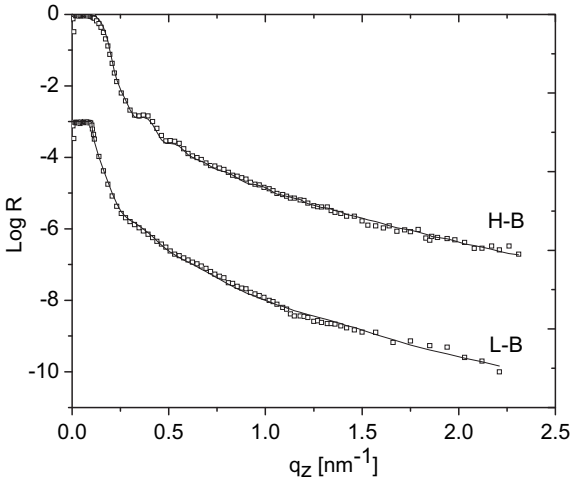

Fig. 5. NR data (symbols) and best fit curves (solid lines) for the H-B and L-B samples after swelling. The curves for the L-B sample have been shifted along the *y*-axis for clarity.

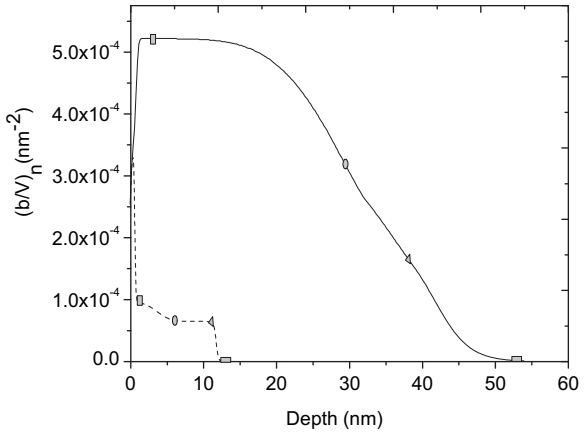

Fig. 6. SLD profiles for the as-deposited (dashed line) and swollen (solid line) sample deposited at high pressure (H–B). Points marked on the two SLD profiles with matching symbols denote points mapped onto one another in the calculation of swelling ratio.

We can use variations in one-dimensional swelling ratio with depth as a measure of how the cross-link density varies. We have estimated the value of one-dimensional swelling ratio as a function of depth and mapped the depth in the swollen film that corresponds to each depth in the dry film. Two main assumptions were used. First, we assumed that the swelling was highly anisotropic, and ignored swelling in the in-plane directions, since covalent bonds with the substrate hinder expansion laterally at the interface with the substrate. This is unimportant as regards the precision with which we can calculate the swelling in the z-direction, because we have measured the total swelling in that direction. However, lateral expansion does occur, and stresses induced by in-plane expansion do play a role in the overall behavior of the film. (In the remainder of the text "swelling ratio" is used to refer to the one-dimensional swelling ratio.) Secondly, we neglected accounting explicitly for the possible presence of air or voids in the film and assumed only two components; polymer and solvent, were present, so that

$$\left(\frac{b}{V}\right)_{i,\text{swollen}} = (1-\phi_{\text{solvent},i}) \times \left(\frac{b}{V}\right)_{i,\text{dry}} + (\phi_{\text{solvent},i}) \times \left(\frac{b}{V}\right)_{\text{solvent}} \tag{2}$$

where the subscript i denotes the ith differential slice of the structure at depth, z_i, from a reference plane. We begin the calculation at the silicon oxide surface ($z = 0$), since the position of the first differential slice of film there does not move, and calculate what the solvent concentration is. Then using this solvent concentration we calculate R_i, the swelling ratio in layer i,

$$\phi_{\text{solvent},i} = 1 - \left(\frac{1}{R_i}\right) \tag{3}$$

and the thickness $\Delta z_{i,\text{swollen}}$, to which the first differential slice of film swelled,

$$\Delta z_{i,\text{swollen}} = \Delta z_{i,\text{dry}} \times R_i. \tag{4}$$

The depths in the swollen film corresponding to depths in the dry film are then calculated by working our way up to the top of the film, making sure that Eqs. (2)–(4) are satisfied self-consistently all through the depth profile. Fig. 8 shows the variation in swelling ratio as a function of depth in the as-deposited ("dry") film. For the film deposited at 0.6 torr pressure, the swelling ratio next to the oxide layer is 10.5 ($\Phi_{\text{solvent}} = 0.91$) and drops sharply to a value of 2 ($\Phi_{\text{solvent}} = 0.50$) and then more slowly through the remainder of film thickness. In contrast, for the film deposited at 0.05 torr pressure, the swelling ratio next to the oxide-interface reaches only 2.4 ($\Phi_{\text{solvent}} = 0.58$) and drops to value of about 1.3 that persists through the rest of the film. The film deposited at high pressure has much lower cross-linking. The presence of cross-linking in the sample deposited at 0.6 torr is consistent with the observation of Jiang and coworkers [34] that such films immersed in acetone (which is not as good a solvent for PP-B as is toluene) did not dissolve. The higher cross-linking density of the films deposited at 0.05 torr is also consistent with the observation, by the same group, that when films deposited at 0.05 torr were swollen with acetone overnight, fragments of film came off the substrate. This is consistent with an argument that for the more highly cross-linked film deposited at lower pressure, higher internal stresses are present. Förch et al. have reported [35] that the reason a highly cross-linked film is more prone to fracture than a loosely cross-linked film is that lateral expansion upon exposure to solvents creates higher internal stresses in highly cross-linked films.

The large difference in cross-linking with pressure could arise from variation in radical concentration with pressure. Plasma polymerization often follows a free-radical mechanism where

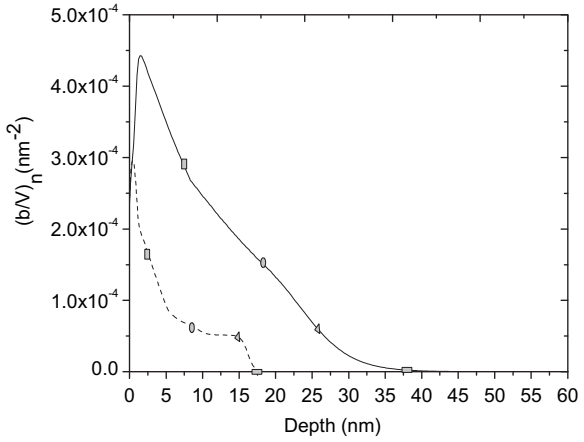

Fig. 7. SLD profiles for the as-deposited (dashed line) and swollen (solid line) sample deposited at low pressure (L–B). Points marked on the two SLD profiles with matching symbols denote points mapped onto one another in the calculation of swelling ratio.

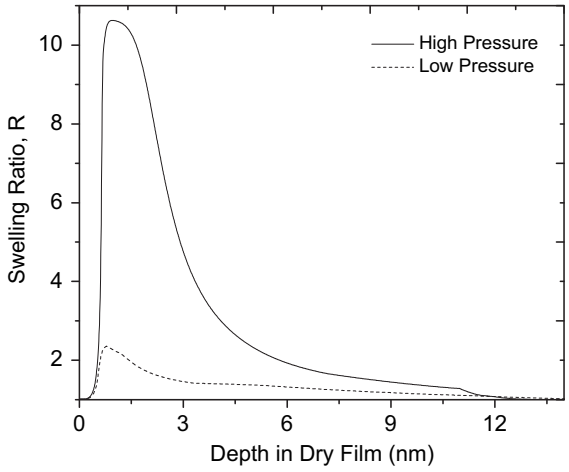

Fig. 8. Swelling ratio with dry depth for PP-B samples deposited at 0.6 and 0.05 torr pressure.

a radical (R*) initiates the process, followed by propagation through reactions with monomers (M), which lead to an ideal polymer:

$$R^* + M \rightarrow R_1^* + M \rightarrow R_2^* + M \rightarrow R_3^* + M \rightarrow \text{Uncross-linked polymer } R_n$$

The competing reaction is:

$$R_j^* + R^* \rightarrow \text{Cross-linked Product.}$$

Based on the above reactions, the amount of cross-linking will then be determined by the ratio of radicals to monomer, [R*]/[M], and [M] is proportional to total pressure. The trend in radical density with pressure is difficult to know, but, in fact, the radical density may decline with increasing pressure due to gas-phase recombination, especially in an afterglow configuration (i.e. with DS feed). Therefore, as the pressure is increased, the ratio [R*]/[M] may decrease since [M] is kept constant through the polymerization, leading to a less cross-linked product.

3.4. Cross-link density comparisons – OFCB monomer

The reflectivity data and best fits for the swollen PP-OFCB samples are shown in Fig. 9 and comparisons of the SLD profiles for each sample are shown in Figs. 10 and 11. The spacing of the fringes decreases with swelling due to the increase in film thickness for both films. The fringe amplitude increases upon swelling for the film deposited at 0.6 torr, while it does not for the film processed at 0.05 torr. This indicates the roughnesses or widths of the interfaces responsible for the fringes do not change with swelling for the film processed at lower pressure, and that the SLD contrasts across those same interfaces change little, if at all, for that film. However, for the film processed at high pressure, the change in amplitude with swelling can be attributed to the greater scattering length density contrast between film and air after swelling with deuterated solvent. X-ray reflectivity (XR) measurements of the films made following the swelling and drying of the films indicated no changes in the films' thicknesses. That is, no material was extracted from the films by the swelling with vapor.

After swelling, the neutron SLD varies with depth in a more pronounced way than for the as-deposited film. If the shape of the SLD profile after swelling paralleled closely the shape before swelling one could infer that the film had swelled uniformly with depth, indicating uniformity in cross-link density with depth. The marked alterations in the shape of the SLD profile upon swelling for both samples indicate that the cross-link density is non-uniform with depth in both films. The larger increase in $(b/V)_n$ with swelling near the substrate indicates much more swelling there, hence a lower cross-link density, than in either the middle or the near-surface region of the film. This behavior is observed for the PP-OFCB films deposited at both pressures. A key finding is that the overall degree of swelling for the PP-OFCB film, 1.4 for H-F and 1.6 for L-F, does not vary much with reactor pressure. However, there are some substantial differences in local values of swelling ratio at different depths in the samples.

Quantitative comparisons of the dry and swollen profiles show that the "transition" layer swells much more for the film deposited at 0.6 torr than for the film deposited at 0.05 torr. Figs. 10 and 11 show the mappings of SLD after swelling to SLD before swelling and Fig. 12 shows how the swelling ratio varies with depth in the dry film for the samples deposited at 0.6 torr and 0.05 torr pressure. The swelling ratio next to the oxide layer reaches 15 ($\Phi_{solvent} = 0.93$) for the film deposited at 0.6 torr and 4 ($\Phi_{solvent} = 0.76$) for the film deposited at 0.05 torr. The depth over which this large swelling is estimated to take place is very small (ca. 1 nm), and is of the order of the depth resolution of a reflectivity measurement made with this range of scattering vector. Therefore, the relative uncertainty of the

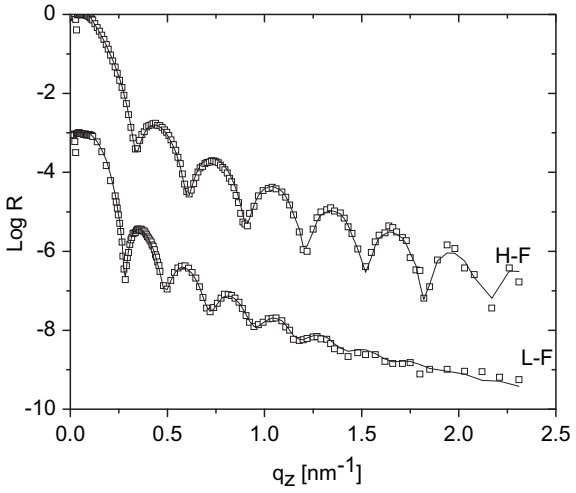

Fig. 9. NR data (symbols) and best fit curves (solid lines) after swelling for PP-OFCB samples deposited using 0.6 torr (H-F) and 0.05 torr (L-F). The pair of curves for the sample deposited using low pressure has been shifted along the *y*-axis for clarity.

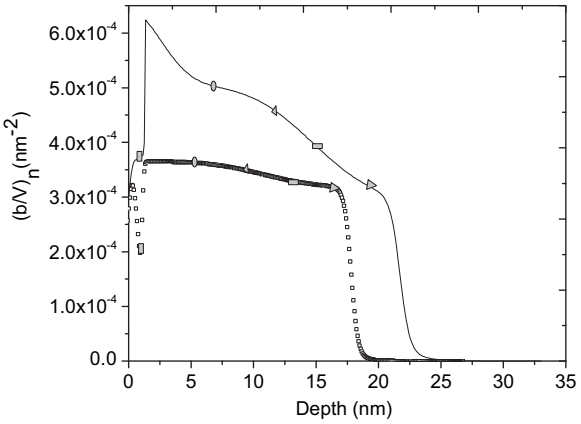

Fig. 10. SLD profiles for the as-deposited (empty squares) and swollen (solid line) PP-OFCB sample deposited at high pressure (H-F).

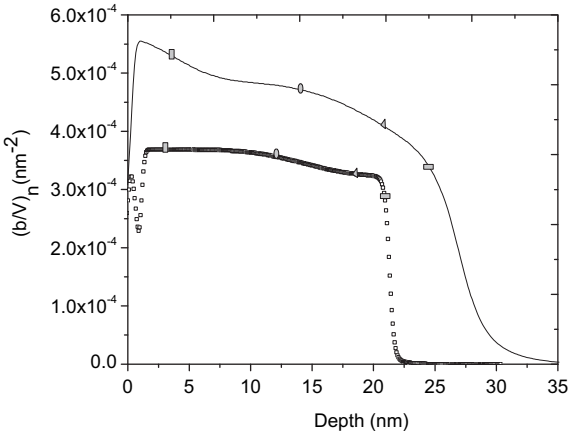

Fig. 11. SLD profiles for the as-deposited (empty squares) and swollen (solid line) PP-OFCB sample deposited at low pressure (L-F).

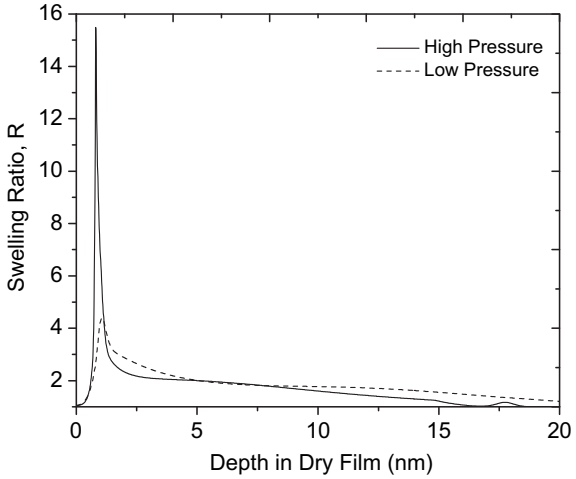

Fig. 12. Variation in swelling ratio with dry depth for PP-OFCB samples deposited at 0.6 (solid line) and 0.05 torr (dashed line).

maximum swelling ratio is much greater than the uncertainty in the swelling ratio elsewhere in the film. The swelling ratio continues to drop as one moves up from the transition layer to the surface, though much less steeply.

For both films there is also a change in cross-link density between the middle of the film and the near-surface region, but the large difference at the substrate interface is the focus of our attention. In the absence of detailed information about how the elemental composition of the film varies with depth, we must be cautious in drawing inferences about the connections between chemistry and the cross-link density. Two observations seem reasonable, however. First, at lower reactor pressure, the impacts of fragments with the substrate surface occur with higher energies. Secondly, in the transition region, immediately adjacent to substrate, the silicon and oxygen atoms in the substrate oxide are available to play a role in building the film structure, whereas farther from the substrate Si and O should be much less important. We conjecture that the higher impact energies at low pressure lead to the higher cross-linking density in the transition region seen for the low pressure PP-OFCB sample. Since the SLD in the dry film changes so rapidly with depth next to the substrate, we know, as pointed out by Kim et al. [9], that the character of the film structure must change markedly as soon as the oxide surface is "masked" by a layer of PP polymer. The result from the swelling measurement makes clear that this rapid change with depth is not only a change in composition (which we can see in part with NR due to the strong contrast for F atoms), but is also a change in cross-linking density. So the cross-linking density may be affected by changes in the degree to which Si and O are incorporated into the structure as well as by changes in the relative abundance of different sorts of C_xF_y groups [36–39]. We close our discussion of the PP-OFCB films by underscoring that for PP-OFCB a change in reactor pressure brings far less change in fragmentation rate than in the case of benzene and therefore the change in overall degree of cross-linking with pressure is much smaller for PP-OFCB as well. In the ultrathin films considered here, the local differences in cross-linking in interfacial regions can play an appreciable role in determining overall film swelling ratio, but for thicker films the overall swelling ratio for PP-OFCB might be effectively unchanged by reactor pressure.

4. Conclusions

For ultrathin PP films, variations in structure with depth near the substrate and near the surface become very apparent, while the structure that is present in the "middle" of such a film is deemphasized. Therefore, using NR, non-uniformities in structure with depth, which provide clues to various facets of the deposition mechanism, become apparent. For the films deposited at 45 W studied here, both a "transition layer" near the substrate [9] and a surface layer of about 7 nm thickness are present for both PP-B and PP-OFCB films.

Changes in reactor pressure at 45 W plasma power lead to much stronger changes in the depth dependent structure for PP-B films than for PP-OFCB films. By measuring the depth distribution of solvent in PECVD films swollen with vapor, unprecedented information about variations in cross-link density with depth and their dependence on processing pressure has been obtained. In particular, the overall cross-linking varies much more strongly with pressure for PP-B films than for PP-OFCB films. For both monomers the cross-link density is lowest next to the substrate where deposition begins. The non-uniformity in swelling ratio is more highly localized and the excursion in swelling ratio value larger for the PP-OFCB films, though overall the PP-OFCB films are more uniform in structure with depth than are the PP-B films. The control of cross-link density and its variation with depth using deposition parameters should be important for optimizing the robustness of PECVD coatings when exposed to potentially damaging solvents. This control could also be used to design the response of PECVD films to environmental stimuli in cases where the films are intended to sense environmental changes.

Acknowledgements

This research was funded by the Collaborative Center for Polymer Photonics (49620-02-1-0428) which is co-funded by the Air Force Office of Scientific Research, Air Force Research Laboratory, and The University of Akron. We acknowledge the support of the National Institute of Standards and Technology, U.S. Department of Commerce, in providing the neutron research facilities used in this work. We thank C. Wolden for helpful comments regarding the polymerization mechanism and John Grant for XPS measurements.

References

[1] Biederman Y. Plasma polymer films. London: Imperial College Press; 2004.
[2] Endo K, Shinoda K, Tatsumi T. J Appl Phys 1999;86(5):2739.
[3] Grant JT, Jiang H, Tullis S, Johnson WE, Eyink K, Fleitz P, et al. Vacuum 2005;80 (1–3):12.
[4] Silverstein MS, Visoly I, Kesler O, Janai M, Cassuto Y. J Vac Sci Technol B 1998;16(6):2957.
[5] Benitez F, Martinez E, Galan M, Serrat J, Esteve J. Surf Coat Tech 2000;125 (2–3):383.
[6] Dilsiz N, Akovali G. Polymer 1996;37(2):333.
[7] Yasuda HK. Plasma polymerization. Orlando: Academic Press; 1985.
[8] Nelson A, Muir WB, Oldham J, Fong C, McLean KM, Hartley PG, et al. Langmuir 2006;22(1):453.
[9] Kim H, Foster MD, Jiang H, Tullis S, Bunning TJ, Majkrzak CF. Polymer 2004;45 (10):3175.
[10] Jeon SH, Wyatt J, Harper-Nixon D, Weinkauf DH. J Polym Sci Part B Polym Phys 2004;42(13):2522.
[11] Kent-Blasie J, Zheng S, Strzalka J. Phys Rev B 2003;67(22):224201.
[12] Lagomarsino S, Di Fonzo S, Jark W, Muller B, Cedola A, Pelka G. Mater Res Soc Symp Proc 2005;382:381.
[13] Benattar JJ, Schalchli A. Phys Scr 1994;50(2):188.
[14] Geer R, Qadri S, Shashidhar R, Thibodeaux FA, Duran SR. Liq Cryst 1994;16 (5):869.
[15] Ziegler E, Ferrero C, Lamy F, Chapron C, Morawe Ch. Adv X-Ray Anal 2002; 45:345.
[16] Zymierska D, Sobczak E, Godwod K, Miotkowska S. Appl Crystallogr 1998; 17:394.
[17] Commercial materials, instruments and equipment are identified in this paper in order to specify the experimental procedure as completely as possible. In no case does such identification imply a recommendation or endorsement by the National Institute of Standards and Technology nor does it imply that the materials, instruments, or equipment identified are necessarily best available for the purpose.

[18] Majkrzak CF, Berk NF, Perez-Salas UA. Langmuir 2003;19(19):7796.
[19] Foster MD. Crit Rev Anal Chem 1993;24(3):179.
[20] Parratt LG. Phys Rev 1954;95:359.
[21] Peri SR, Kim H, Akgun B, Enlow J, Jiang H, Bunning TJ, Li X, Foster MD, submitted for publication.
[22] Morosoff N, Haque R, Clymer SD, Crumbliss AL. J Polym Sci Part A Polym Chem 1985;3(6):2098.
[23] Engleman RA, Yasuda HK. Polym Mater Sci Engr 1990;62:19.
[24] Gengenbach TR, Chatelier RC, Vasic ZR, Griesser HJ. Polym Prep (Am Chem Soc Div Polym Chem) 1993;34:687.
[25] Gengenbach TR, Vasic ZR, Chatelier RC, Griesser HJ. J Polym Sci Part A Polym Chem 1994;32(8):1399.
[26] Gengenbach TR, Chatelier RC, Griesser HJ. Surf Interface Anal 1996;24(4):271.
[27] Gengenbach TR, Chatelier RC, Griesser HJ. Surf Interface Anal 1996;24(4):611.
[28] Gengenbach TR, Griesser HJ. Polymer 1999;40(18):5079.
[29] Kuzuya M, Ito H, Kondo S, Noda N, Noguchi A. Macromolecules 1991;24 (25):6612.
[30] Kuzuya M, Noguchi A, Ito H, Kondo S, Noda N. J Polym Sci Part A Polym Chem 1991;29(1):1.
[31] Kuzuya M, Noguchi A, Ishikawa M, Koide A, Sawada K, Ito A, et al. J Phys Chem 1991;95(6):2398.
[32] Kuzuya M, Morisaki K, Niwa J, Yamauchi Y, Xu K. J Phys Chem 1994;98 (44):11301.
[33] Jiang H, Grant JT, Enlow J, Su W, Bunning TJ. J Mater Chem 2009;19(15):2234.
[34] Jiang H, Hong L, Venkatasubramanian N, Grant JT, Eyink K, Wiacek K, et al. Thin Solid Films 2007;515(7–8):3513.
[35] Förch R, Zhang Z, Knoll W. Plasma Processes Polym 2005;2(5):351.
[36] Kim Y, Lee J, Kim K. J Vac Sci Technol A 2009;27(4):900.
[37] Zheng L, Ling L, Hua X, Oehrlein GS, Hudson EA. J Vac Sci Technol A 2005;23 (4):634.
[38] Garrison MD, Luginbühl R, Overney RM, Ratner BD. Thin Solid Films 1999;352 (1):13.
[39] Favia P, Perez-Luna VH, Boland T, Castner DG, Ratner BD. Plasmas Polym 1996;1(4):299.